

Detection of Individual Gas Molecules by Graphene Sensors

F. Schedin^{1,2}, K.S. Novoselov¹, S.V. Morozov^{1,3}, D. Jiang¹, E.H. Hill², P. Blake², & A.K. Geim¹

¹School of Physics and Astronomy and ²School of Computer Sciences,
University of Manchester, M13 9PL, Manchester, UK

³Institute for Microelectronics Technology, 142432 Chernogolovka, Russia

The ultimate aspiration of any detection method is to achieve such a level of sensitivity that individual quanta of a measured value can be resolved. In the case of chemical sensors, the quantum is one atom or molecule. Here we report graphene-based devices that are capable of detecting minute concentrations of various active gases and allow us to discern individual events when a molecule attaches to the sensor's surface.

Solid-state gas sensors are renowned for their high sensitivity, which – in combination with low production costs and miniature sizes – have made them ubiquitous and widely used in many applications (1,2). Recently, a new generation of gas sensors have been demonstrated using carbon nanotubes and semiconductor nanowires (3-9). The high acclaim received by such sensors is, to a large extent, due to their exceptionally high sensitivity allowing detection of toxic gases in concentrations as small as 1 part per billion (ppb). This and even higher levels of sensitivity are sought for industrial, environmental and military monitoring (6-9). In this report, we show that graphene can be heavily doped by both electrons and holes through its exposure to various chemicals and that gas sensors made from graphene (10) offer the ultimate sensitivity, being able to detect individual molecules attaching to a micron-size sensitive area of a graphene device.

The operational principle of the reported sensors is based on changes in their resistivity due to molecules absorbed by graphene layer and acting as donors or acceptors (1-9). The exceptional sensitivity arises due to the unique nature of this strictly two-dimensional material that offers a whole combination of features important for solid state gas sensors. First, graphene essentially has only a surface and no volume, which maximizes the effect caused by surface dopants. Second, graphene is highly conductive, having few crystal defects and exhibiting metallic conductivity even in the limit of zero carrier concentrations (10-12). Third, graphene allows four-probe measurements on a single-crystal chip with electrical contacts that are purely Ohmic and have low resistance. These features combine to minimise an intrinsic (excess) noise (13), which should normally conceal changes caused by individual absorbed dopants.

The studied graphene devices were prepared by micromechanical cleavage of bulk graphite at the surface of oxidized Si wafers as described in (11). This allowed us to obtain monocrystalline patches of graphene of typically ten microns in size. By using electron-beam lithography, we made electrical (Au/Cr) contacts to graphene and then defined multiterminal Hall bars by etching graphene in an oxygen plasma. The microfabricated devices (upper inset in Fig. 1a) were placed in variable temperature insert inside a superconducting magnet and fully characterised by using field-effect measurements (10-12) at temperatures T from 4 to 400K and in magnetic fields B up to 12T, which allowed us to find mobility μ of charge carriers (typically, $\approx 5,000 \text{ cm}^2/\text{Vs}$ at 300K) and distinguish between single-, bi- and few-layer devices (12), in addition to complementary measurements of their thickness carried out by optical and atomic force microscopy (10-12). The lower inset of Fig. 1a shows an example of the field-effect behaviour exhibited by our devices at room T . By applying positive (negative) gate voltages V_g between the Si wafer and graphene, we induced electrons (holes) in graphene in concentrations $n = \alpha \cdot V_g$. The coefficient $\alpha \approx 7.2 \cdot 10^{10} \text{ cm}^{-2}/\text{V}$ was found from Hall effect measurements, in agreement with the geometry of the resulting capacitor for a 300 nm layer of SiO_2 (10-12). One can see from this plot that longitudinal and Hall resistivity (ρ_{xx} and ρ_{xy} , respectively) are (anti)symmetric functions of V_g . ρ_{xx} exhibits a peak at zero V_g whereas ρ_{xy} simultaneously

passes through zero, which shows that the transition from electron to hole transport occurs at zero V_g indicating that graphene is in its pristine, undoped state (12,14).

To assess the graphene devices as gas sensors, the insert was evacuated and then connected to a relatively large (5 litre) glass volume containing a selected chemical strongly diluted in pure helium at atmospheric pressure. Figure 1b shows the response of zero-field resistivity $\rho = \rho_{xx}(B=0)$ to NO_2 , NH_3 , H_2O and CO in concentrations C of 1 part per million (ppm). One can see large, easily detectable changes in ρ , which occurred within 1 min and, for the case of NO_2 , practically immediately after letting the chemicals in. The initial rapid response was followed by a region of saturation, in which the resistivity changed relatively slowly. We attribute this region to redistribution of absorbed gas molecules between different surfaces in the insert. After an equilibrium state was reached, we evacuated the container again, which led only to small and slow changes in ρ (region III in Fig. 1b), indicating that absorbed molecules were strongly attached to the graphene devices at room T . Nevertheless, we found that the initial undoped state could be recovered relatively easily by annealing the devices at 150°C in vacuum for a few minutes (region IV). A short-time UV illumination was found to offer an alternative to thermal annealing.

To gain more information about the observed chemical response, we simultaneously measured changes in ρ_{xx} and ρ_{xy} caused by gas exposure, which allowed us to find directly concentrations Δn of chemically induced charge carriers (see Fig. 1) and their sign. The Hall measurements revealed that NO_2 , H_2O and iodine acted as acceptors whereas NH_3 , CO , ethanol and PMMA were donors. Importantly, we found that chemical doping caused only small changes in mobility $\mu = \rho_{xy}/\rho_{xx}B$ and, therefore, the response in $\rho = 1/ne\mu$ was mainly due to changes in n rather than in the scattering rate due to absorbed dopants acting as additional impurities. This allowed us to achieve the linear resistive response with respect to chemical doping over a large range of C . To this end, we electrically biased our devices (by more than $\pm 10\text{V}$) to higher-concentration regions, in which both longitudinal ($\sigma = 1/\rho$) and Hall conductivities ($\sigma_{xy} = 1/\rho_{xy} = ne/B$) were proportional to n (10-12). In this regime, changes in σ and σ_{xy} were found proportional to concentration C of an examined chemical, which greatly simplifies the use of graphene gas sensors in practical terms.

The detection limit for solid state gas sensors is usually defined as the minimal concentration that causes a signal exceeding the sensors' intrinsic noise (1-9). In this respect, a typical level of intrinsic resistance fluctuations in our devices was below 1 Ohm (13,15) which, for example, for the device in Fig. 1 translates into the detection limit of several ppb. Selected devices (15) (in particular, those made from few-layer graphene) exhibited 100 times lower noise, allowing the detection of NO_2 and NH_3 at a level of well below 1 ppb (see further), which rivals the best sensitivities demonstrated previously for gas sensors (1-9). Moreover, we found that, unlike many other sensors, graphene devices did not exhibit saturation in the detected signal with time at small C ; that is, the effect of chemical doping in our case is essentially cumulative. In the particular experiment shown in Fig. 1b, the saturation observed in region II was found to be caused by a limited amount of gas molecules able to reach the micron-sized sensitive area, because of the competition with other large absorbing areas, in agreement with theory of chemical detectors of a finite size (16). Figure 2 illustrates the accumulation effect by showing changes in ρ_{xx} and ρ_{xy} as a function of exposure time t for the same sensor but exposed to a constant flow of NO_2 and NH_3 (in ppm concentrations) rather than to the chemicals' limited volumes. In this case, graphene's doping continued increasing with t (in contrast to the experiment shown in Fig. 1) because of the continuous supply of active molecules into the sensitive area. Within an hour, the device's resistivity changed by 300%. Longer exposure or higher C allowed us to reach a doping level up to $\approx 10^{13}\text{cm}^{-2}$, which then remained constant at room T for many days. Note that the behaviour in Fig. 2 clearly resembles the corresponding dependences in Fig. 1a but charge carriers are now induced by chemical rather than electric-field doping. The found accumulation effect yields that the detection limit can be exceedingly small for long exposure times, allowing a sufficient amount of gas molecules to be absorbed within the sensitive area.

To demonstrate the fundamental limit for the sensitivity of graphene gas sensors, we exposed our devices to a vanishingly small leak of strongly diluted NO_2 chosen so that ρ remained nearly constant over several minutes. In this regime, chemically-induced changes in ρ were no longer smooth but occurred in a series of small steps (see Fig. 3). If we closed the leak and started evacuating the sample space, similar steps

occurred in the opposite direction. To maximize the signal-to-noise ratio in these measurements, we optimized our measurements (15). The optimum size of graphene Hall bars was found to be $\approx 1\mu\text{m}$. Smaller devices exhibited stronger resistance fluctuations, whereas larger sizes lead to smaller changes in resistivity. Also, we employed the Hall geometry in the regime of very low carrier concentrations ($<10^{11}\text{cm}^{-2}$) (15). This allowed us to minimise the sensitive area to the central region of the Hall cross and, at the same time, to calibrate the steps in ρ_{xy} directly in terms of electron charge transfer by comparing the chemically-induced signal with the known response to gate voltage. The latter is especially important for the low-concentration region where there is no simple relation between ρ_{xy} and n . To cause changes in ρ_{xy} of the same height δR as the steps in the inset of Fig. 3, we found that it required changes in V_g of $\approx 1.5\text{mV}$, which corresponds to $\Delta n \approx 10^8\text{cm}^{-2}$ and translates into one electron charge e removed from the Hall cross' area of $1\times 1\mu\text{m}^2$ in size (note that changes in ρ_{xy} as a function of V_g were smooth; that is, no charge quantization occurred in the devices' transport characteristics – as expected). Measurements in other B yielded the same result: a typical step size δR during the chemical exposure corresponded to $\approx e$. As a reference, we repeated the same measurements but without exposure to NO_2 and found no steps.

For statistical analysis, we recorded a large number of curves such as that in the inset of Fig. 3. The resulting histograms (≈ 100 hours on continuous recording) with and without exposure to NO_2 are plotted in Fig. 3. The reference curves (no NO_2) exhibited many small (positive and negative) steps, which gave rise to a “noise peak” at small δR . Large steps were rare. On the contrary, the exposure to slowly-leaking NO_2 led to many large steps. The steps were not equal in size, as expected, because gas molecules could be absorbed anywhere including fringes of the sensitive area, which results in varying contributions. Moreover, because of a finite time constant used in the measurements (1 sec), random resistance fluctuations could overlap with individual steps either enhancing or reducing the latter, and different steps could also overlap occasionally (like the first step in the inset of Fig. 3, which has a double height). The corresponding histogram shows the same “noise peak” but, in addition, the statistical distribution is now significantly broader due to an additional maximum that is centred at $\delta R \approx 0.05\text{Ohm}$ and corresponds to removing approximately one electron from the detection area. This leaves no doubt that the observed changes during chemical exposure were quantized with each event signalling the absorption of a single NO_2 molecule.

The described experiments imply that the absorption of NO_2 is accompanied by a charge transfer of $1e$ between the sea of conduction electrons and an absorbed molecule. At first sight, this is surprising because NO_2 molecules absorbed on graphene are expected to provide a “charge transfer” of only $\approx 0.1e$ (17-19). However, the latter term comes from physical chemistry and refers to the polarization of a chemical bond between NO_2 and carbon and, if dopants create an impurity band, each dopant has to contribute exactly one electron (c.f., shallow donors in Si have “charge transfer” close to zero). Also, note that individual doping events were observed only in the low-concentration regime ($<10^{11}\text{cm}^{-2}$), in which graphene edges could provide a sufficient number of absorption sites so that the doping did not need to occur at graphene's surface. Indeed, broken bonds at plasma-etched edges are considered as favourite absorption sites and can provide much larger charge transfer (20-23). More generally, the mechanism of chemical doping in graphene can be expected to be similar to the one for carbon nanotubes. Unfortunately, the latter remains unexplained and still controversial, being attributed to either bulk doping (3,17,24) or changes in contact resistance (25,26). Also, it is believed that the presence of the SiO_2 substrate can be important for chemical sensing in carbon nanotubes. Our four-probe measurements certainly rule out any effect originating from electrical contacts but we cannot exclude an influence of the substrate. Furthermore, hydrocarbon residues on graphene's surface are practically unavoidable, and we believe that they can effectively “functionalize” graphene, acting as both absorption sites and intermediaries in charge transfer.

To conclude, graphene-based chemical sensors offer the ultimate sensitivity such that individual toxic molecules can be detected. Large arrays of such sensors would increase the catchment area and allow detection of chemical gases in as minute concentrations as practically desirable. The epitaxial growth of few-layer graphene wafers (27,28) offers a realistic promise of mass production for such sensor networks. Equally important (29,30) is the demonstrated possibility of chemical doping of graphene by both electrons and holes in very high concentrations. This should allow microfabrication of p - n junctions, which attract

significant interest from the point of view of both fundamental physics and applications. Despite its short history, graphene is considered to be a very promising material for electronics by academic and industrial researchers (28-30), and the possibility of its chemical doping improves further the prospects of graphene-based electronics.

1. P. T. Moseley, *Meas. Sci. Technol.* **8**, 223 (1997).
2. S. Capone *et al*, *J. Optoelect. Adv. Mater.* **5**, 1335 (2003).
3. J. Kong *et al*, *Science* **287**, 622 (2000).
4. P. G. Collins, K. Bradley, M. Ishigami, and A. Zettl, *Science* **287**, 1801 (2000).
5. P. Qi *et al*, *Nano Lett.* **3**, 347 (2003).
6. L. Valentini *et al*, *Appl. Phys. Lett.* **82**, 961 (2003).
7. J. P. Novak *et al*, *Appl. Phys. Lett.* **83**, 4026 (2003).
8. J. Li *et al*, *Nano Lett.* **3**, 929 (2003).
9. D. Zhang *et al*, *Nano Lett.* **4**, 1919 (2004).
10. K.S. Novoselov *et al*, *Science* **306**, 666 (2004).
11. K.S. Novoselov *et al*, *Proc. Natl Acad. Sci. USA* **102**, 10451 (2005).
12. K.S. Novoselov *et al*, *Nature* **438**, 197 (2005).
13. P. Dutta and P. M. Horn, *Rev. Mod. Phys.* **53**, 497 (1981).
14. M.S. Dresselhaus and G. Dresselhaus, *Adv. Phys.* **51**, 1 (2002).
15. We employed low-frequency (30 to 300 Hz) lock-in measurements and used relatively high driving currents of $\approx 100 \mu\text{A}/\mu\text{m}$. The latter suppressed any voltage noise, so that the remaining resistance fluctuations were intrinsic and due to switching of unstable defects (13). Such defects are known to lead to 1/f-noise, which fundamentally limits the sensitivity of all thin-film charge detectors. Graphene devices were found to exhibit an exceptionally low level of intrinsic noise (as compared to any other detector based on charge sensitivity), which can be attributed to high crystal and electron-transport quality of graphene (10-12). The lowest noise was found in devices with highest mobility ($>10^4 \text{ cm}^2/\text{Vs}$) and lowest contact resistance R_c . Sensors made from few-layer (3 to 5) graphene were somewhat electrically quieter, probably because their R_c could be as low as $\approx 100 \text{ Ohm}$, as compared with typically $\approx 1 \text{ kOhm}$ for single-layer devices. As a good indicator of sufficiently low noise we used the possibility to detect changes in ρ or ρ_{xy} with varying gate voltage by $\approx 1 \text{ mV}$. This corresponds to changes of less than one elementary charge e inside the sensitive area of the Hall cross of $1 \times 1 \mu\text{m}^2$ in size. We tested various regimes to maximize the sensitivity, and the maximum signal-to-noise ratio was found in the region of low doping ($<10^{11} \text{ cm}^{-2}$; $|V_g| < 1 \text{ V}$). In this region, the noise in ρ was not at its lowest but this was compensated by the steepest response in Hall resistivity to an induced electric charge (lower inset in Fig. 1a). The low intrinsic noise is the fundamental reason for the achieved exceptional sensitivity, and this also shows that graphene devices can be employed in other applications where ultra-sensitive local probes of magnetic field, electric charge, etc. are required.
16. P.E. Sheehan and L.J. Whitman, *Nano Lett.* **5**, 803 (2005).
17. H. Chang, J. D. Lee, S. M. Lee, and Y. H. Lee, *Appl. Phys. Lett.* **79**, 3863 (2001).
18. S. Santucci *et al*, *J. Chem. Phys.* **119**, 10904 (2003).
19. A.J. Bennett, B. McCarroll, and R. P. Messmer, *Phys. Rev. B* **3**, 1397 (1971).
20. Y.J. Xu and J.Q. Li, *Chem. Phys. Lett.* **400**, 406 (2004).
21. X. Feng *et al*, *J. Am. Chem. Soc.* **127**, 10533 (2005).
22. J. Andzelm, N. Govind, N. Maiti, *Chem. Phys. Lett.* **421**, 58 (2006).
23. J.A. Robinson *et al*, *Nano Lett.* **6**, 1747 (2006).
24. K. Bradley, J. P. Gabriel, M. Briman, A. Star, and G. Grüner, *Phys. Rev. Lett.* **91**, 218301 (2003).
25. S. Heinze *et al*, *Phys. Rev. Lett.* **89**, 106801 (2002).
26. J. Zhang *et al*, *Appl. Phys. Lett.* **88**, 123112 (2006).
27. I. Forbeaux, J.-M. Themlin, and J.-M. Debever, *Phys. Rev. B* **58**, 16396 (1998).
28. C. Berger *et al*, *Science* **312**, 1191 (2006).
29. C. Zhou, J. Kong, E. Yenilmez, and H. Dai, *Science* **290**, 1552 (2000).
30. B. Obradovic *et al*, *Appl. Phys. Lett.* **88**, 142102 (2006).

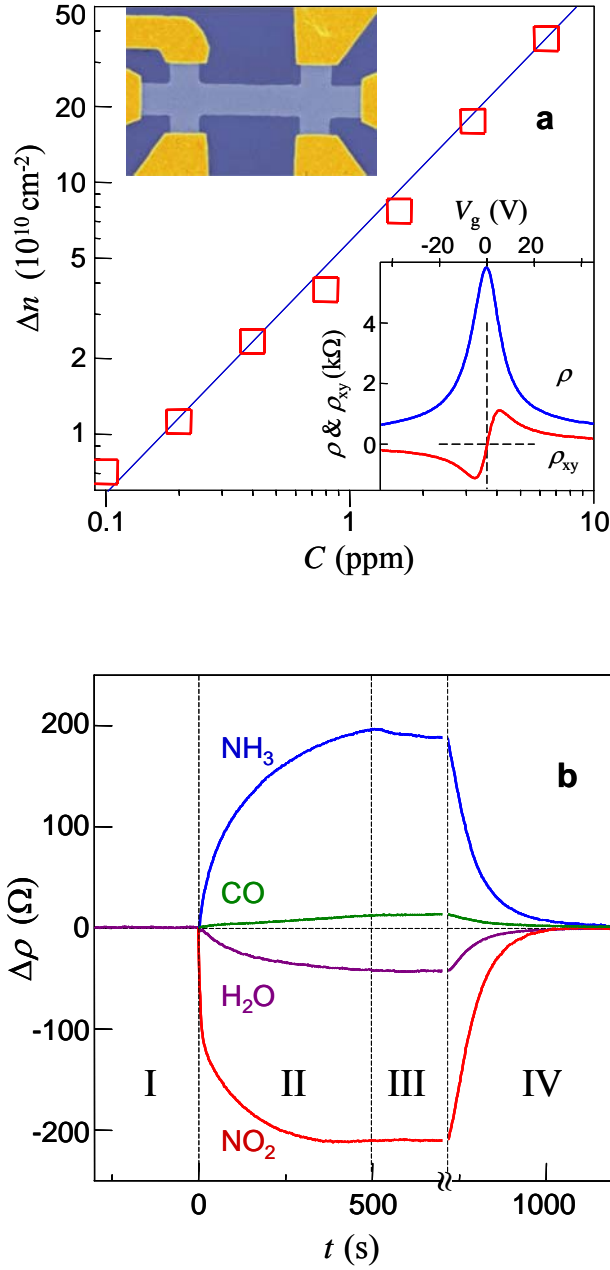


Figure 1. Chemical sensitivity of graphene. (a) – Concentration Δn of chemically-induced carriers in a single-layer graphene sensor exposed to different concentrations C of NO_2 . Upper inset: scanning-electron micrograph of this device (in false colour). The scale of the micrograph is given by the width of the Hall bar, which is $1\mu\text{m}$. Lower inset: Characterisation of graphene sensors by using the electric field effect. To measure the Hall effect, $B = 1\text{T}$ was applied perpendicular to graphene's surface. (b) – Changes in zero-field resistivity of single-layer devices caused by their exposure to various active gases diluted in concentration 1 ppm. The positive (negative) sign of changes in ρ is chosen here to indicate electron (hole) doping. To distinguish between chemical gases acting as donors and acceptors, we measured the sign of the Hall effect. Region I – the device is in vacuum prior to its exposure; II – exposure to a 5 l volume of a diluted chemical; III – evacuation of the experimental setup; and IV – annealing at 150°C . The response time was limited by our gas-handling system and a few-second delay in the lock-in measurement circuit. Note that the annealing caused an initial spike-like response in ρ , which lasted for a few minutes and was generally irreproducible. For clarity, this transient region between III and IV is omitted, as indicated in the figure.

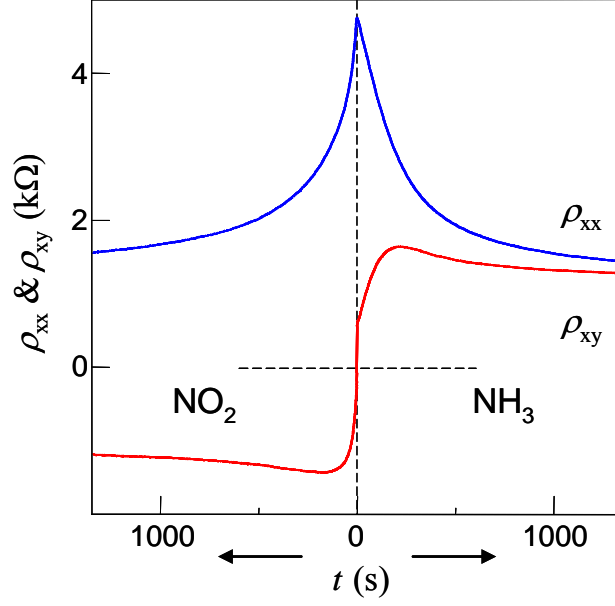


Figure 2. Accumulation of dopants on graphene. Changes in the longitudinal and Hall resistivity of graphene exposed to a continuous supply of strongly-diluted NH_3 (right part of the figure). After the exposure, the device was again annealed close to the undoped state and then exposed to NO_2 in the same fashion (left part). Here, measurements of both ρ_{xx} and ρ_{xy} were carried out in field $B=1\text{T}$.

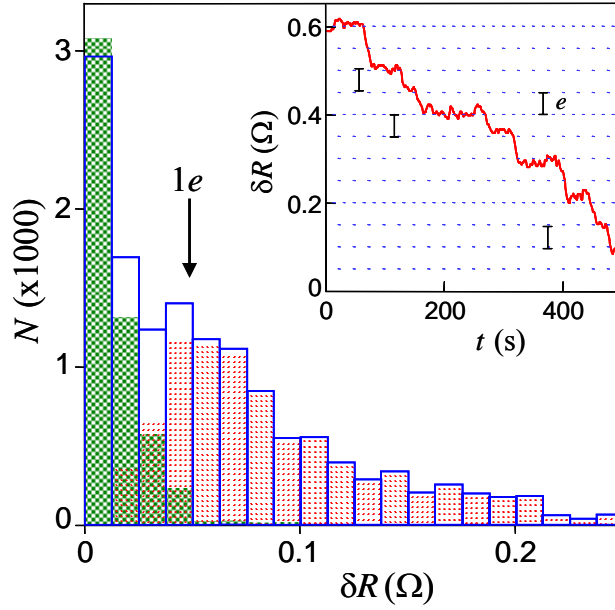


Figure 3. Single-molecule detection by graphene sensors. Inset: step-like changes in ρ_{xy} observed in the low-concentration regime ($<10^{11}\text{cm}^{-2}$; $|V_g|<1\text{V}$) during exposure to extremely diluted NO_2 . A typical step size (in this particular case, $\Delta R \approx 0.05\text{ Ohm}$; $B=4\text{T}$) corresponds to removal of approximately one electron from the sensitive area ($1 \times 1\mu\text{m}^2$) of the graphene device. Main panel: Statistical distribution of step heights ΔR with and without gas exposure (open bars and green shaded areas, respectively). The difference between the two is shown in semi-transparent red. For this analysis, all changes in ρ_{xy} larger than 0.01 Ohm and quicker than 5s (lock-in's time constant was 1s) were registered as individual steps. The “noise peak” was symmetric with respect to negative and positive steps. Only the steps in one direction are plotted.